Title

Complementary modulation of BMP signaling improves bone healing efficiency.

Authors

Fan, Jiabing
Zhang, Xiao
Kang, Minjee
et al.

Publication Date

2023-11-01

DOI

10.1016/j.biomaterials.2023.122335

Peer reviewed

HHS Public Access

Author manuscript

Biomaterials. Author manuscript; available in PMC 2024 November 01.

Published in final edited form as:

Biomaterials. 2023 November ; 302: 122335. doi:10.1016/j.biomaterials.2023.122335.

Complementary Modulation of BMP Signaling Improves Bone Healing Efficiency

Jiabing Fan, MD, PhD[1,2], **Xiao Zhang, PhD**[1], **Minjee Kang, PhD**[1], **Chung-Sung Lee, PhD**[1,3], **Lauren Kim**[1], **Danny Hadaya**[4], **Tara L. Aghaloo, DDS, MD, PhD**[4,*], **Min Lee, PhD**[1,5,*]

[1]Division of Advanced Prosthodontics, School of Dentistry, University of California, Los Angeles, California 90095

[2]Department of Pharmaceutical Sciences, School of Pharmacy and Health Professions, University of Maryland Eastern Shore, Princess Anne, Maryland 21853

[3]Department of Pharmaceutical Engineering, Soonchunhyang University, Asan, Chungcheongnam-do, Korea (Republic of) 31538

[4]Division of Diagnostic and Surgical Sciences, School of Dentistry, University of California, Los Angeles, California 90095

[5]Department of Bioengineering, University of California, Los Angeles, California 90095

Abstract

The bone morphogenetic protein (BMP) signaling pathway plays a crucial role in bone development and regeneration. While BMP-2 is widely used as an alternative to autograft, its clinical application has raised concerns about adverse side effects and deteriorated bone quality. Therefore, there is a need to develop more sophisticated approaches to regulate BMP signaling and promote bone regeneration. Here, we present a novel complementary strategy that targets both BMP antagonist noggin and agonist Trb3 to enhance bone defect repair without the application of exogenous BMP-2. *In vitro* studies showed that overexpression of Trb3 with simultaneous noggin suppression significantly promotes osteogenic differentiation of mesenchymal stem cells. This was accompanied by increased BMP/Smad signaling. We also developed sterosome nanocarriers, a non-phospholipid liposomal system, to achieve non-viral mediated noggin suppression and Trb3 overexpression. The gene-loaded sterosomes were integrated onto an apatite-coated polymer scaffold for *in vivo* calvarial defect implantation, resulting in robust bone healing compared to BMP-2 treatments. Our work provides a promising alternative for high-quality bone formation by regulating expression of BMP agonists and antagonists.

[*]**Corresponding authors:** Tara L. Aghaloo, DDS, MD, PhD, Division of Diagnostic and Surgical Sciences, UCLA School of Dentistry, 10833 Le Conte Avenue, CHS 53-009, Los Angeles, CA 90095-1668, Telephone: (310) 206-6766, Fax: (310) 825-7232, taghaloo@dentistry.ucla.edu; Min Lee, PhD, Division of Advanced Prosthodontics, UCLA School of Dentistry, 10833 Le Conte Avenue, CHS 23-088F, Los Angeles, CA 90095-1668, Telephone: (310) 825-6674, Fax: (310) 825-6345, leemin@ucla.edu.

AUTHOR CONTRIBUTIONS

J.F. conceived and designed the experiments, conducted experiments, collected and/or assembled data, analyzed and interpreted data, and wrote the manuscript. X.Z, M. L, C.L and L. K fabricated and analyzed the scaffolds. D. H and T.L.A performed animal surgeries and interpreted data. M.L conceived and designed the study and analyzed and interpreted data.

COMPETING INTERESTS STATEMENT

The authors indicated no potential conflicts of interest.

Keywords

Noggin; Trb3; BMP Signaling; Sterosome; Bone Repair

1. INTRODUCTION

Impaired bone healing and regeneration are a significant challenge in large orthopedic and oral and maxillofacial bone defects, particularly following severe trauma, chronic bone loss diseases, and tumor resection.[1] Autologous bone grafts are considered the gold standard treatment, but their limited availability and associated morbidities hamper their widespread use.[2-4] While allografts represent a commonly used alternative, their implementation is associated with risks such as immunological reactions, disease transmission, and infection.[2-4] To overcome these barriers, recent promising therapeutic alternatives are toward using synthetic bone graft substitutes and osteoinductive factors.

Bone morphogenetic protein (BMP) signaling is critical for craniofacial development and morphology, and its disruption can result in severe abnormalities.[5-7] BMP signaling is tightly regulated by both extracellular and intracellular agonists and antagonists.[5-7] While BMPs have shown remarkable potential for bone regeneration, their safety and efficacy profiles are not completely established and their increased clinical use brings more concerns regarding complications associated with high dosage requirements, inappropriate delivery systems, and off-label use as well as a risk of cancer development.[8-10] Therefore, developing alternative therapeutic strategies that complement BMP signaling activity is necessary for more effective and safe bone regeneration.

Extracellularly, BMP activity is controlled through various BMP antagonists.[11] Noggin, in particular, is one of the most prominent BMP antagonists that specifically binds BMPs and inhibits their osteoinductive function.[11] In response to BMPs, cells increase noggin expression as a negative feedback mechanism to prevent excessive BMP signaling.[12] Exogenous use of noggin resulted in impaired bone formation, while suppression of noggin exerted a significant increase in bone growth.[13-15] In addition to extracellular BMP antagonists, intracellular BMP mediators also play a crucial role in regulating BMP signaling and osteogenic potential. Trb3, a member of the tribbles family of pseudokinases, is involved in various metabolic functions and cellular differentiation processes.[16-20] Our recent work discovered that Trb3 promoted osteogenic potential of MSCs and inhibited adipogenic differentiation.[21] Trb3 also has been found to be a potent BMP agonist and increase endogenous BMP signaling by interacting with Smad4. However, this led to increased expression of BMP antagonist noggin.[22] Thus, the potency of Trb3 in BMP pathways can be enhanced by downregulation of BMP antagonists. Taken together, these results suggest that augmentation of Trb3 expression (BMP agonist) combined with suppression of noggin (BMP antagonist) could maximize endogenous BMP signaling activity and promote effective bone regeneration without exogenous BMP applications.

Nanoparticles have shown great potential for delivering therapeutic genes and drugs for tissue regeneration and disease treatment.[23] Among the various nanoparticle types, liposomes are one of the most studied nanovesicles and have been clinically adopted

as a drug delivery carrier due to their versatile structure and high biocompatibility.[24-26] However, conventional phospholipid-based liposomes suffer from poor stability, limiting their application.[27] To address this, a new class of liposomes (sterosomes) was designed using non-phospholipid single chain amphiphiles and high content of cholesterol.[28,29] These sterosomes have significantly increased nanoparticle stability with very low permeability, making them a promising candidate for nucleic acid/drug delivery.[28,29] Recent studies have demonstrated the efficacy of sterosomes in the delivery of various osteogenic genes and small molecules, further emphasizing their potential for bone tissue regeneration.[30]

Here, we developed a sterosome composed of palmitic acid and cholesterol, functionalized with bone-binding alendronate, and loaded Trb3- and noggin-directed nucleic acids (Figure 1). The constructed nanoparticulate sterosomes were incorporated onto an apatite-coated poly (lactic-co-glycolic acid) (Ap-PLGA) scaffold for *in vivo* bone defect implantation (Figure 1). The osteogenic effect of Trb3 delivery combined with noggin suppression was evaluated in MSCs *in vitro*, and its bone formation capacity was further measured in a critical-sized mouse calvarial defect model. The quality of bone healing was also assessed in comparison with a standard BMP-2 treatment. Our findings suggest a new therapeutic strategy for sophisticated regulation of BMP signaling and high-quality bone regeneration.

2. MATERIALS AND METHODS

2.1 Cell Culture and Transduction

The mouse mesenchymal stem cells (mMSCs) were harvested from bone marrow of adult C57BL/6 mice (JAX) and cultured in DMEM medium with 10% FBS and 1% Penicillin-Streptomycin (Invitrogen, CA) as previously described.[31] Lentiviral particles carrying full-length Trb3 and noggin shRNA (Vectorbuilder, IL) were used to transfect the cells, aiming to inhibit noggin expression and overexpress Trb3. The resulting transfected cells were utilized for subsequent in vitro studies.

2.2 RNA Extraction and qRT-PCR

Total RNA was extracted from the cells using Trizol reagent (Life Technologies) and the RNeasy Mini kit (Qiagen, CA), following the manufacturer's protocol.[32] Complementary DNA was synthesized from an aliquot of 500 ng RNA per sample, using the SuperScriptTM III First-Strand Synthesis System (Life Technologies). qRT-PCR analysis was performed using a 20 μL SYBR Green reaction system on a LightCycler 480 PCR instrument (Roche, IN), with GAPDH as the internal control for normalizing the expression of each target gene. The primer sequences for all genes are listed in supplementary Table 1.

2.3 ALP Stain/Activity and Alizarin Red Stain

To evaluate the osteogenic potential of the transfected MSCs in vitro, they were cultured in osteogenic medium (OM, Sigma, MO) consisting of DMEM, 10% FBS, 50 μg/mL L-ascorbic acid, 10 mM β-glycerophosphate, and 100 nM dexamethasone. To assess the expression of alkaline phosphatase (ALP), the transfected MSCs were fixed in 10% formalin at specific time points and then stained using the ALP colorimetric kit (Sigma), which includes Nitro Blue tetrazolium, 5-Bromo-4-chloro-3-indoxylphosphate, and AP

buffer. ALP activity was analyzed by digesting the cells in NP-40 lysis buffer (Life Technologies), incubating them in a buffer containing p-nitrophenol phosphate substrate (Sigma), measuring the absorbance at 405 nm using a plate reader, and normalizing the values to the whole DNA content, which was measured using a PicoGreen dsDNA kit (Invitrogen). To detect mineral deposition, the cells were stained with 2% alizarin red solution (Sigma) and visualized using an Olympus IX71 microscope. Mineralized extracellular matrix produced by the cells was further quantitatively analyzed by dissolving it in 10% (v/v) acetic acid and measuring the absorbance at a wavelength of 405 nm.

2.4 Western-blot Assay

The western blot assay was performed according to previously described methods.[32] Briefly, cells were washed with PBS, harvested, and lysed in 0.2% NP40 cell lysis buffer (Thermo Fisher). The resulting protein lysates were separated by Sodium Dodecyl Sulfate-Polyacrylamide Gel Electrophoresis (SDS-PAGE) and transferred to Immobilon polyvinyl difluoride (PVDF) membranes (Millipore, MA). The membranes were then incubated with primary antibodies specific to Trb3, noggin, pSMAD1/5/8, or GAPDH (Santa Cruz Biotechnology, CA). After washing, the membranes were incubated with secondary antibodies conjugated with Horseradish Peroxidase (HRP) (Millipore, MA) and visualized using chemiluminescent HRP (Denville Scientific, NJ). The resulting images were quantitatively analyzed using Image J (NIH).

2.5 Luciferase Assay

The Id1 luciferase reporter assay was conducted following the manufacturer's instructions. The cells were seeded in a 12-well plate and allowed to reach 70-80% confluence. Next, cells were co-transfected with the pGL4 [luc2P/hID1/Hygro] vector and the Renilla control vector (Promega) using Lipofectamine 2000 (Invitrogen). After incubating for 6 hours, the transfection medium was replaced with growth medium and cells were allowed to incubate for an additional 48 hours. Luciferase activities were measured using the dual-luciferase reporter system (Promega) and the values were normalized to those of the Renilla internal control.

2.6 Preparation of Sterosome Nanoparticles

Sterosomes were fabricated by self-assembly of cholesterol and palmitic acid using an ultrasonic method. First, a solution of cholesterol/palmitic acid (molar ratio: 7/3) was dissolved in benzene/methanol (volume ratio: 9/1) and then hydrated with Tris-NaCl buffer (50 mM Tris, 140 mM NaCl, pH 7.4). To obtain multilamellar vesicles, the suspensions were mixed, heated to 70°C, and frozen at −80°C for up to five cycles. Sterosomes were then generated under ultrasound conditions (using a high-power 500 W sonic dismembrator with a 20 s on, 5 s off, 20% amplitude, 25 W mm−2 power intensity) for 20 min. To generate apatite binding sterosomes, 4.3 mg of total lipid of sterosome in 1 mL of 50 mM Tris-NaCl buffer solution was combined with 385 μg of EDC and 450 μg of NHS, and allowed to react for 4 hours. To achieve a 5% modification rate, 208 μg of alendronate was introduced and the reaction was continued for 24 h. To remove un-conjugated alendronate, EDC, and NHS, the suspension was further purified by size exclusion chromatography using Sephadex G-50. To form guanidine-rich sterosomes, a mixture of 2.5 mg of alendronate-modified

sterosome and 1.15 mg of DMTMM along with 1.8 mg of agmatine was incubated in 1.3 mL of 50 mM Tris-NaCl buffer solution for 24 h at room temperature and purified using size exclusion chromatography. pDNA (Vectorbuilder, Chicago, IL) was then complexed with PEI at an N/P ratio of 10. The mass ratio of pDNA to sterosomes was 1/7.5. Next, the pDNA/PEI complex was added to the sterosome solution and mixed using a vortex for 1 min. The pDNA/PEI complex was finally assembled into the core of sterosomes under ultrasound conditions for 1 min. The size and zeta potential of the sterosomes were determined using a Malvern Zetasizer, while their morphology was observed using Cyro-TEM (TF-20). To assess the transfection efficiency, mMSCs were transfected with pGFP using PEI or sterosomes. After 48 hours of transfection, GFP expression was observed under a fluorescent microscope. Cell viability was further analyzed using the AlamarBlue assay (Invitrogen).

2.7 Intracellular Tracking

To analyze intracellular tracking, a complex at N/P 10 was formed using FITC-labeled PEI and Cy5-labeled pDNA. Subsequently, MSCs were seeded into glass-bottomed dishes with $1x10^4$ cells per well. After 24 hours of culture, the cells were incubated with either sterosomes nanoparticles (300 ng Cy5-labeled pDNA per well) in culture medium containing 10% FBS or pDNA/PEI complex in culture medium without FBS. Following 1 and 12 hours of incubation, the cells were washed with PBS and stained with LysoTracker blue. Confocal laser scanning microscopy (CLSM) was used to image the cells with the FITC channel (green, ex 480 nm and em 530 nm), Cy5-labeled pDNA channel (red, EX 633 nm and EM 670 nm), LysoTracker-stained lysosome channel (blue, EX 405 nm and EM 422 nm).

2.8 Preparation of Scaffold

Ap-PLGA scaffolds were fabricated using a solvent casting and leaching process, following our previously established methods.[33] First, a PLGA/chloroform solution was mixed with sucrose (200-300 μm diameter) to achieve a porosity of 92% (volume fraction). The mixture was then compressed into Teflon molds and freeze-dried overnight at 100 mTorr and −110°C (SP Industries, Inc.). The resulting scaffolds were immersed in double-distilled (dd) H2O to wash away the sucrose. Next, the PLGA scaffolds were coated with an apatite layer by incubating them in simulated body fluid (SBF). To enhance the adhesion of the apatite layer, the scaffolds were subjected to glow discharge argon plasma etching (Harrick Scientific, Pleasantville, NY). The etched scaffolds were then incubated in SBF1 (containing CaCl2, MgCl2·6H2O, NaHCO3, K2HPO4·3H2O, Na2SO4, KCl, and NaCl) for 24 h, followed by incubation in SBF2 (containing CaCl2, K2HPO4·3H2O, KCl, and NaCl) for another 24 h at 37°C. Finally, the Ap-PLGA scaffolds were incorporated with sterosomes for further experiments. The morphology of the resulting sterosomes/Ap-PLGA complex was observed using scanning electron microscopy (SEM) (Nova NanoSEM 230, FEI, OR).

2.9 Apatite Binding Assay

Sterosomes were labeled with a fluorescent dye by adding 5-FAM (67.2 μg) with EDC (385 μg) and NHS (450 μg) to sterosome solution (4.3 mg) and allowed to react for 24 h. The labeled sterosome suspension was subsequently purified using size exclusion

chromatography via Sephadex G-50. Subsequently, 50 μL of 5-FAM-labelled sterosomes (100 μg/mL) were loaded onto the surface of an Ap-PLGA scaffold measuring 5 mm in diameter. The resulting sterosome/scaffold complex was dissolved in Tris-NaCl buffer at the indicated time, and the mixture was collected and centrifuged (at 12,000 rpm for 1 min). The supernatant was then measured using a microplate reader with an excitation wavelength of 480 nm and an emission wavelength of 530 nm.

2.10 Cellular differentiation on sterosome/Ap-PLGA scaffold

To evaluate the osteogenic potential of cells on the scaffolds, mMSCs were seeded onto sterosome/Ap-PLGA scaffolds (5 mm in diameter and 1 mm in height) at a density of 1 x 10^5 cells/scaffold. The cells were stained with a Live/Dead staining kit (Invitrogen) for 15 minutes and then imaged under an Olympus IX71 microscope at days 1, 7, and 14 to assess viability. The AlamarBlue assay kit (Invitrogen) was used to quantify cell proliferation on the cell/scaffold complex. Osteogenic differentiation was measured by culturing sterosome-laden scaffolds incorporated with mMSCs in osteogenic media (OM) and analyzing them with real-time PCR, ALP stain, and alizarin red stain at the indicated time points.

2.11 Mouse calvarial defect models

The animal surgery was conducted in strict adherence to the Guidelines for the Care and Use of Laboratory Animals of the National Institutes of Health, and the protocols were approved by the UCLA Animal Research Committee. CD-1 nude mice (mixed sex, 8-12 weeks old, Charles River) were used to create the critical-sized calvarial defect model following the methods previously established by our group.[33] The calvaria of the mice underwent trephine drilling with constant irrigation, and 3-mm full-thickness craniotomy defects were created in each parietal bone without injuring the underlying dura mater. Ap-PLGA scaffolds (3 mm in diameter and 1 mm in height) alone or with sterosomes were placed onto the calvarial defects before suturing. BMP-2 control groups were prepared by adsorbing BMP-2 onto Ap-PLGA scaffolds at a final protein concentration of 100 μg/mL (700 ng/scaffold). After surgery, all animals were allowed to fully recover from anesthesia on a warm sheet and were then transferred to the vivarium for postoperative care. Analgesia was administered via subcutaneous injections of 0.1 mg/kg buprenorphine for 3 days postoperatively, and the animals received drinking water containing trimethoprim–sulfamethoxazole for 7 days to prevent potential infection.

2.12 Microcomputerized tomography (microCT) scanning

After collection from experimental mice, the calvarial tissues were fixed with 4% formaldehyde and stored in 70% ethanol for subsequent imaging analysis. A high-resolution microcomputed tomography scanner (SkyScan 1172, Belgium) was used to scan the tissue samples, with settings at 57 kVp, 184 μA, 0.5 mm aluminum filtration, and 10 μm resolution. The samples were scanned, and the data were visualized and three-dimensionally reconstructed using Dolphin 3D software (Dolphin Imaging & Management Solutions, CA). The new bone area and volume were measured using ImageJ software (NIH) and CTAn (SkyScan), respectively. Bone-specific analysis included new bone area/original defect area (percent area), new bone volume/total volume (BV/TV), bone mineral density (BMD), and trabecular number (Tb.N)/thickness (Tb.Th).

2.13 Histological and immunohistochemical analyses

After fixation, the tissues were decalcified using 10% ethylenediaminetetraacetic acid (EDTA) and embedded in paraffin, followed by cutting into 5 μm sections. The resulting sections were then deparaffinized using xylene and subjected to staining with hematoxylin and eosin (H&E) solution as well as Masson's trichrome kit (Sigma) to visualize new bone formation, which appeared light blue. Furthermore, to detect osteoclasts, the deparaffinized slides underwent a TRAP stain. Polarizing light microscopy was employed to image the sections stained with 0.1% PicroSirius red solution (Polysciences, PA). Immunohistochemical analysis was performed by incubating the deparaffinized sections with anti-PPARγ antibodies (Santa Cruz) followed by staining using the HRP/DAB detection kit (Abcam). Finally, the sections were counterstained with Mayer's hematoxylin (Abcam), and ImageJ software was used for colorimetric analysis.

2.14 Statistical analysis

The study's quantitative data were presented as mean ± SD, with statistical significance defined as *$p < 0.05$, **$p < 0.01$, ***$p < 0.001$, and ****$p < 0.0001$. When comparing two groups, a two-tailed Student's t-test was used for parametric data analysis. Meanwhile, for comparisons of more than two groups, a one-way ANOVA analysis of variance was employed, followed by a post hoc Tukey's test to compare the two groups. GraphPad PRISM software (v6.0, CA) was utilized for all statistical analyses.

3. RESULTS

3.1 Combined effect of noggin suppression with Trb3 overexpression on MSC osteogenesis

Increasing evidence suggests that regulating BMP antagonists and agonists can mediate the osteogenic commitment of MSCs.[13,21] Our previous studies have shown that inhibiting BMP antagonists, such as noggin, can promote stem cell osteogenic differentiation and bone repair, while targeting BMP agonists, such as Trb3, promotes osteogenesis.[14,22] In this study, we investigated the combined effect of noggin suppression and Trb3 overexpression on osteogenic differentiation of MSCs *in vitro*.

To down-regulate noggin expression and up-regulate Trb3 expression, we transfected MSCs with lentiviral particles encoding noggin shRNA and/or full-length Trb3. We then evaluated the expression levels of osteogenic genes and proteins in transfected MSCs. Our results showed that the combination of noggin suppression and Trb3 overexpression significantly increased MSC osteogenesis, as evidenced by significant elevation in the expression levels of osteogenic genes (including *Osterix, Runx2, ALP*, and *Osteocalcin (OCN)*), the expression of ALP measured by ALP stain/activity, and mineral deposition detected by Alizarin Red stain/quantification, compared to MSCs treated with noggin shRNA or Trb3 alone and control groups (Figure 2a-e). The osteogenic gene expression in the combined treatment groups (noggin suppression + Trb3 overexpression) was comparable or superior to MSCs treated with BMP-2 (100 ng/ml) (supplementary Figure 1). Overall, these findings indicate that the combined treatment of noggin suppression with Trb3 overexpression has an additive or synergistic effect on the osteogenic commitment of MSCs.

3.2. Stimulation of BMP/Smad signaling by combined treatment of noggin suppression and Trb3 overexpression

To further elucidate the mechanisms underlying the enhanced MSC osteogenesis by noggin suppression and Trb3 overexpression, we evaluated the expression of BMP/Smad signaling using various molecular approaches *in vitro.* We first assessed the expression of noggin and Trb3 at the gene and protein level using real-time PCR and western blot assays, respectively, and confirmed successful suppression of noggin and overexpression of Trb3 (Figure 3a, b). We then detected a significant increase of pSmad1/5/8 in MSCs treated with noggin suppression and Trb3 overexpression compared to other treatment groups (Figure 3b), suggesting that the combination treatment promotes endogenous BMP/Smad signaling. Furthermore, we observed a significant increase in Id1 gene expression and promoter activity, a direct target of BMP/Smad signaling, in MSCs treated with noggin suppression and Trb3 overexpression (Figure 3a, c).

To validate the role of BMP/Smad signaling in the increased MSC osteogenesis, we treated MSCs with a small molecule BMP inhibitor (LDN193189) in control, noggin suppression, Trb3 overexpression, or noggin suppression and Trb3 overexpression groups. We examined ALP expression using ALP stain/quantification and found that the implementation of BMP signaling inhibitor reversed the increased osteogenesis of MSCs treated with noggin suppression, Trb3 overexpression, or combination, and reduced the ALP expression level to that of MSCs treated with control (Figure 3d, e).

Overall, our findings suggest that the combination of noggin suppression and Trb3 overexpression promotes MSC osteogenesis by stimulating endogenous BMP/Smad signaling, providing a basis for the development of translational approaches for bone repair and regeneration through targeting BMP antagonists/agonists.

3.3 Development of nanoparticulate sterosomes for delivery of noggin shRNA and Trb3

The modulation of BMP agonists/antagonists has shown great potential for enhancing MSC osteogenic commitment and bone repair, but a lack of safe and efficient delivery vehicles has been a key barrier to gene therapy. Here, non-phospholipid nanoparticulate sterosomes were employed as stable delivery vehicles. Sterosomes were constructed through self-assembly of cholesterol and palmitic acid. The carboxyl groups of sterosomes were then decorated with apatite binding alendronate via a condensation reaction. To increase their cell-penetrating ability, the residual carboxyl groups were further functionalized with agmatine, a member of primary amino compounds (guanidines), to create a positive surface charge. Finally, the core of the modified sterosomes was incorporated with complex of PEI/pDNA encoding noggin shRNA and full length Trb3.

TEM images and dynamic light scattering data demonstrated that the created sterosomes displayed unilamellar nanostructures with an average size of ~100 nm (Figure 4a). The zeta potential of sterosomes was increased from −19.5 to 17.9 mV after the conjugation of guanidine groups. Gene loading did not significantly alter these properties. The transfection efficiency of sterosomes was evaluated using GFP as a reporter gene. The data showed that approximately 80% of cells expressed GFP, which is higher than gold standard PEI groups,

indicating high transfection efficiency (Figure 4b). In addition, cell treated with sterosomes showed high viability over 90%, while cell viability was decreased after the treatment with PEI groups (Figure 4c). The intracellular fate of sterosomes in MSCs was examined using fluorescein FITC-labeled PEI and Cy5-labeled pDNA. CLSM images showed lysosomal entrapment of sterosome particles after 1 hour of incubation, but the particles were observed to escape from lysosomes after 12 hours of incubation (supplementary Figure 2).

To make nanoparticulate sterosomes suitable for local bone defect repair, Ap-PLGA scaffolds were created as an osteoconductive substrate for cellular adhesion and to bind sterosome nanoparticles. SEM revealed highly porous and interconnected pore morphology with typical plate-like structures of apatite on the scaffold struts (Figure 4d). Incorporating sterosome nanoparticles into Ap-PLGA scaffolds did not significantly alter the porous structure as evaluated by micro-CT analysis (supplementary Figure 3). To assess the binding efficiency of sterosome nanoparticles to the apatite-coated scaffolds, 5-FAM labeled nanoparticles were loaded onto the scaffolds. Fluorescence images showed strong binding of alendronate-modified sterosomes compared to unmodified sterosome resulting from high affinity between the alendronate groups in the nanoparticles and the calcium-containing apatite layers of Ap-PLGA scaffolds (Figure 4e). Moreover, the binding efficiency of alendronate-modified sterosomes was substantially increased over time. Sterosome binding was further confirmed by a cholesterol assay and a higher amount of sterosome cholesterol was detected on Ap-PLGA scaffolds compared to non-apatite coated scaffolds (supplementary Figure 4).

3.4 Enhanced osteogenesis of sterosome-laden scaffolds *in vitro*

Before evaluating the potential of the sterosome-laden Ap-PLGA scaffold to bone repair *in vivo*, we further conducted *in vitro* studies on its osteogenic properties. First, we examined the cellular proliferation in the sterosome-laden scaffolds. MSCs were seeded on scaffolds incorporated with or without sterosome nanoparticles and analyzed using Live/Dead stain and AlamarBlue assay (Figure 4f, g). All experimental groups exhibited high levels of cellular viability over the 14-day culture period, indicating that the sterosome-laden scaffolds remained highly biocompatible for cellular growth.

We also investigated the ability of sterosome-laden scaffolds to induce osteogenic differentiation (Figure 5). To this end, we analyzed the expression of osteogenic genes in MSCs seeded on the scaffolds at day 3. Consistent with our 2D results, scaffolds laden with sterosome encapsulating pDNA encoding Trb3 and noggin shRNA showed additive effects on the expression of osteogenic genes, including *Runx2, Osterix, ALP*, and *OPN* (Figure 5e). Moreover, the increased osteogenesis of MSCs cultured on the gene activated scaffolds was evidenced by elevated ALP expression and mineralization, when compared to scaffolds loaded with sterosomes encapsulating pDNA encoding Trb3 or noggin shRNA alone, or control pDNA (Figure 5a-d).

Overall, the sterosome-laden Ap-PLGA scaffold displayed high cellular viability and effective osteogenic induction, demonstrating its potential for *in vivo* bone defect treatment.

3.5 Sterosome-laden scaffolds show potential for *in vivo* bone defect repair

We investigated the efficacy of implanting sterosome-laden Ap-PLGA scaffolds for *in vivo* bone repair using a mouse critical-sized calvarial defect model. The calvarial tissues were collected 8 weeks postoperatively and imaged using high resolution microCT (Figure 6) to evaluate sterosome/scaffold-mediated bone healing.

The microCT images revealed that the scaffold laden with sterosome encapsulating pDNA encoding Trb3 and noggin shRNA resulted in substantially greater bone healing compared to the treatment groups encapsulating pDNA encoding Trb3 or noggin shRNA alone while control scaffolds induced only minimal bone healing (Figure 6a). Quantitative analysis of the microCT scan showed up to ~90% bone healing in the treatment group of noggin suppression and Trb3 overexpression, in contrast to only ~10% in the control, ~55% in noggin suppression, and ~57% in Trb3 overexpression. The significant enhancement of new bone formation by noggin suppression + Trb3 overexpression was quantitatively confirmed with increased bone volume, trabecular number, and bone mineral density (Figure 6b). The measured bone volume fraction was in a comparable range to those of gold standard bone grafting or BMP-2 treatment previously reported in similar defect models.[34-36]

Histological and immunohistochemical analyses further validated the substantial bone healing in the treatment of noggin suppression + Trb3 overexpression. H&E and Masson trichrome stains showed a large amount of newly formed compacted bone with mature collagen matrices as observed by Picrosirus red stains in the combined treatment groups (Figure 6c).

3.6 High quality of bone healing *in vivo*

To investigate the effectiveness of noggin suppression + Trb3 overexpression for bone healing, we compared this combined approach with a treatment using BMP-2, which is an FDA-approved growth factor commonly used for bone repair and regeneration in clinical settings. In this study, we used Ap-PLGA scaffolds loaded with BMP2 (100 μg/mL) previously established for mouse calvarial defect repair as a comparative control group.

Calvarial bone defect healing was evaluated at eight weeks after the surgery. microCT imaging showed significant bone healing in both treatment groups (Figure 7a). Quantitative analysis of the new bone area indicated that the defects treated with sterosome/scaffold constructs delivering noggin shRNA + Trb3 had ~90% bone healing while BMP-2 treatment groups had 85% bone healing (Figure 7b). Furthermore, the combined treatment group exhibited a higher BV/TV (~38%) in comparison to the BMP-2 treatment group (~33%). The analysis of trabecular bone morphology revealed thicker and more numerous trabeculae in the defects treated with gene activated scaffolds than in those treated with BMP-2 (Figure 7b).

In addition, histological analysis showed that the treatment of noggin suppression + Trb3 overexpression resulted in higher quality bone healing with highly aligned collagen fibers as observed by Picrosirus red staining and a lower presence of adipocytes and osteoclasts detected by immunohistochemical staining of PPARγ and TRAP, respectively (Figure 7c). By contrast, BMP-2 treatment groups led to regenerative areas with increased adipocytes

and osteoclasts. Our results suggest that the sterosome-laden scaffold mediating Trb3 expression and noggin suppression presents a promising bone graft substitute to promote high quality bone formation and efficacious bone healing.

4. DISCUSSION

In this study, we developed a complementary bone formation approach by regulating BMP agonists and antagonists to maximize the potency of endogenous BMP signaling and osteogenic differentiation (Figure 1). To translate our combined approach to the treatment of craniofacial bone defects, we employed sterosome nanocarriers to deliver therapeutic genes and immobilized them onto an apatite-coated polymer scaffold (Figure 1). The high quality of bone healing mediated by the nanoparticle/scaffold construct was detected in a calvarial defect model, posing a promising therapeutic alternative to conventional treatment for bone defects.

BMPs exert widely recognized roles in bone growth during mammalian development.[5,8] BMP-2 is the most extensively studied osteoinductive factor and has been clinically exploited to promote bone repair and regeneration.[10,37] BMP-2 administers its pro-osteogenic effect by enhancing dimerization of specific receptors, resulting in the phosphorylation of Smad1/5/8 intermediates and ultimately modulating transcriptional activity.[8] Although BMP-2 exhibits clinical efficacy in osseous repair, adverse clinical events such as fat-filled void bone, osteoclastic bone resorption, extreme edema/inflammation, and uncontrolled ectopic bone often occur.[10] These limitations further necessitate a new therapeutic strategy for the careful regulation of BMP signaling.

The activities of BMP signaling have been found to be regulated by a variety of BMP agonists and antagonists.[38] Targeting either BMP agonists or antagonists has been well studied in MSC lineage commitment and bone repair/regeneration.[15,21,22] Nonetheless, few investigations have been conducted on the combined effect of simultaneous regulation of BMP agonists and antagonists in ossification. In the current work, we upregulated BMP agonist Trb3 with simultaneous suppression of BMP antagonist noggin to maximize BMP signaling and bone defect repair without the application of exogenous BMP-2. Noggin has been reported to be a specific antagonist of BMPs that regulate BMP activity and osteogenic differentiation, while Trb3 acted as a novel BMP agonist in the stimulation of BMP/Smad signaling and associated osteogenesis.[11,22] Moreover, Trb3 was found to inhibit adipogenesis and inflammation.[20,21,39-41] Deteriorated bone quality and surrounding soft tissue swelling observed in BMP-2 treatment have been suggested to be closely related to increased adipogenesis and inflammatory reactions.[10] Investigations have indicated that shifting of the balance between osteogenesis and adipogenesis in MSCs may result in abnormal bone formation.[42] In addition, our prior studies demonstrated that Trb3 overexpression in MSCs by genetic manipulation led to elevated expression of noggin.[22] Together with these results, the combined use of noggin suppression and Trb3 overexpression was expected to complement endogenous BMP signaling activity and result in efficacious bone healing. Nearly complete bone healing was observed in the calvarial defect model by co-delivery of noggin shRNA + Trb3, while delivery of noggin shRNA or

Trb3 alone only resulted in partial bone healing. Furthermore, the quality of bone healing was superior to that of standard BMP-2 treatment.

We applied 100 μg/mL BMP-2 for comparison because the dose was found to be the most effective to induce bone formation in our previous study.[21,33] The current effective BMP-2 dose for human use is approved at 1.5 mg/mL. However, increasing doses of BMP-2 above 100 μg/mL did not result in higher bone healing, but instead induced cystic bone formation with excessive adipogenesis in our previous rodent bone defect models.[21,22] Ectopic bone formation was reported when clinical BMP-2 dose was used in a similar calvarial defect.[43] Because many of the side effects of BMP-2 is dose-related, we employed PLGA scaffolds with biomimetic apatite coating designed to deliver BMP-2 in a sustained manner without the premature protein release observed with current collagen carriers (supplementary Figure 5). The dose-dependent adverse effect, however, was observed with the scaffold. Our complementary strategy of noggin suppression + Trb3 overexpression is expected to maximize endogenous BMP signaling in bone regeneration and may serve as efficacious adjuncts to BMP therapy to reduce BMP-2 dose or potentially eliminate the requirement of exogenous recombinant BMP-2.

Viral vectors are commonly used vehicles for delivering specific genes into target cells.[39-41] However, the use of viral vectors for gene transfer is still limited by non-specific targeting and genotoxicity.[44-46] In the past decade, lipid-based nanoparticles such as liposomes has made significant progress as pharmaceutical delivery vehicles but early liposomal systems are limited by insufficient stability.[47] We recently developed a new type of liposomes (sterosomes) with high sterol content that exhibited significantly increased nanoparticle stability and gene transfection efficiency compared to conventional phospholipid liposomes.[48] In this study, nanoparticles were prepared by self-assembly of high amount of cholesterol (70 mol%) with palmitic acid as a single chain amphiphile and loaded with pDNA that simultaneously encodes full-length Trb3 and noggin shRNA. In addition, carboxyl groups from the single chain amphiphile allow versatile modification of sterosome surface. We modified the sterosome surface with bone binding alendronate and positively charged guanidine moieties. The alendronate modification enhances binding affinity of sterosomes to mineralized surfaces,[49] while the guanidine-rich sterosomes improve cellular penetration. The modified sterosomes showed high cellular uptake and transfection efficiency, and successfully immobilized onto an apatite layer of 3D scaffolds. Bisphosphonates (e.g. alendronate) bind to hydroxyapatite crystals of bone with a strong affinity. By taking advantage of this distinctive interaction, previous studies demonstrated the stable binding of bisphosphonate-functionalized nanoparticles or liposomes onto various biomaterial scaffolds incorporating hydroxyapatites.[50,51] pDNA loaded in the modified sterosomes exhibited a sustained release from Ap-PLGA scaffolds (supplementary Figure 5) and promoted mesenchymal cell osteogenesis over 28 days. These nanoparticulate sterosomes may be versatile tools to treat systemic bone diseases or local bone defects when systemically administrated or integrated with bone graft materials.

5. CONCLUSIONS

This study presents a new complementary molecular strategy targeting a BMP antagonist/agonist to enhance endogenous BMP signaling and promote osteogenic differentiation of MSCs by regulating expression of noggin and Trb3. The use of a nonviral sterosomal gene delivery nanoparticles integrated with porous biomaterial scaffolds resulted in significant bone healing in a mouse calvarial defect model compared to a BMP-2 as a positive control. These findings suggest that the complementary regulation of BMP signaling could serve as a promising alternative to current BMP therapeutics, with potential implications for the treatment of large skeletal defects in a more effective and safe manner.

Supplementary Material

Refer to Web version on PubMed Central for supplementary material.

ACKNOWLEDGEMENTS

This work was supported by grants from the National Institutes of Health (R01 DE027332 to M.L. and R03 DE030539 to J.F.), the Department of Defense (W81XWH-18-1-0337 to M.L.), MTF Biologics (to M.L.) and Osteo Science Foundation (to J.F.).

DATA AVAILABILITY

Data will be made available on request.

REFERENCES

1. Broyles JM, Abt NB, Shridharani SM, Bojovic B, Rodriguez ED, et al. (2014) The fusion of craniofacial reconstruction and microsurgery: a functional and aesthetic approach. Plast Reconstr Surg. 134(4):760–9. [PubMed: 25357035]
2. Plum AW, Tatum SA. (2015) A comparison between autograft alone, bone cement, and demineralized bone matrix in cranioplasty. Laryngoscope. 125(6):1322–7. [PubMed: 25641743]
3. Broyles JM, Abt NB, Shridharani SM, Bojovic B, Rodriguez ED, et al. (2014) The fusion of craniofacial reconstruction and microsurgery: a functional and aesthetic approach. Plast Reconstr Surg. 134(4):760–9. [PubMed: 25357035]
4. Elsalanty ME, Genecov DG. (2009) Bone grafts in craniofacial surgery. Craniomaxillofac Trauma Reconstr. 2(3):125–34. [PubMed: 22110806]
5. Salazar V, Gamer L, Rosen V. (2016) BMP signaling in skeletal development, disease and repair. Nature reviews endocrinology. 12:203–221.
6. Graf D, Malik Z, Hayano S, Mishina Y. (2016) Common mechanisms in development and disease: BMP signaling in craniofacial development. Cytokine Growth Factor Rev. 27:129–39. [PubMed: 26747371]
7. Wang R, Green J, Wang Z, Deng Y, Qiao M, et al. (2014) Bone Morphogenetic Protein (BMP) signaling in development and human diseases. Genes & Diseases. 1:17–105.
8. Urist MR. (1965) Bone morphogenetic proteins. Science. 150:893. [PubMed: 5319761]
9. Thies RS, Bauduy M, Ashton BA, Kurtzberg L, Wozney JM, et al. (1992) Recombinant Human Bone Morphogenetic protein-2 Induces Osteoblastic Differentiation in W-20-17 Stromal Cells. Endocrinology. 130, 1318–1324. [PubMed: 1311236]
10. James A, Lachaud G, Shen J, Asatrian G, Nguyen V, et al. (2016) A Review of the Clinical Side Effects of Bone Morphogenetic Protein-2. Tissue Eng Part B Rev. 22(4): 284–97. [PubMed: 26857241]

11. Warren SM, Brunet LJ, Harland RM, Economides AN, Longaker MT. (2003) The BMP Antagonist Noggin Regulates Cranial Suture Fusion. Nature. 422: 625–629 [PubMed: 12687003]
12. Gazzerro E, Gangji V, Canalis E. (1998) Bone Morphogenetic Proteins Induce the Expression of Noggin, Which Limits Their Activity in Cultured Rat Osteoblasts. J. Clin. Investig 102: 2106–2114. [PubMed: 9854046]
13. Heliotis M, Tsiridis E. (2008) Suppression of bone morphogenetic protein inhibitors promotes osteogenic differentiation: therapeutic implications. Arthritis Res Ther. 10(4):115. [PubMed: 18710600]
14. Fan J, Park H, Tan S, Lee M. (2013) Enhanced osteogenesis of adipose derived stem cells with Noggin suppression and delivery of BMP-2. PLoS One. 8(8):e72474. [PubMed: 23977305]
15. Wan DC, Pomerantz JH, Brunet LJ, Kim JB, Chou YF, et al. (2007) Noggin suppression enhances in vitro osteogenesis and accelerates in vivo bone formation. J Biol Chem. 282(36):26450–9. [PubMed: 17609215]
16. Qi L, Heredia JE, Altarejos JY, Screaton R, Goebel N, et al. (2006) TRB3 links the E3 ubiquitin ligase COP1 to lipid metabolism. Science. 312, 1763–1766. [PubMed: 16794074]
17. Avery J, Etzion S, DeBosch BJ, Jin X, Lupu TS, et al. (2010) TRB3 function in cardiac endoplasmic reticulum stress. Circ. Res 106:1516–1523. [PubMed: 20360254]
18. van de Peppel J, Strini T, Tilburg J, Westerhoff H, van Wijnen AJ, van Leeuwen JP. (2017) Identification of three early phases of cell-fate determination during osteogenic and adipogenic differentiation by transcription factor dynamics. Stem Cell Reports. 8:947–960. [PubMed: 28344004]
19. Staines KA, Zhu D, Farquharson C, MacRae VE. (2014) Identification of novel regulators of osteoblast matrix mineralization by time series transcriptional profiling. J Bone Miner Metab. 32:240–51. [PubMed: 23925391]
20. Takahashi Y, Ohoka N, Hayashi H, Sato R. (2008) TRB3 suppresses adipocyte differentiation by negatively regulating PPARgamma transcriptional activity. J Lipid Res. 49(4):880–92. [PubMed: 18187772]
21. Fan J, Pi-Anfruns J, Guo M, Im DCS, Cui ZK, et al. (2017) Small molecule-mediated tribbles homolog 3 promotes bone formation induced by bone morphogenetic protein-2. Sci Rep. 7:7518. [PubMed: 28790361]
22. Fan J, Lee CS, Kim S, Zhang X, Pi-Anfruns J, et al. (2021) Trb3 Controls Mesenchymal Stem Cell Lineage Fate and Enhances Bone Regeneration by Scaffold-Mediated Local Gene Delivery. Biomaterials 264:120445. [PubMed: 33069136]
23. Torchilin VP (2005) Recent Advances with Liposomes as Pharmaceutical Carriers. Nat. Rev. Drug Discovery 4:145–160. [PubMed: 15688077]
24. Immordino ML, Dosio F, Cattel L (2006) Stealth Liposomes: Review of the Basic Science, Rationale, and Clinical Applications, Existing and Potential Int. J. Nanosci 2006: 297–315.
25. Bozzuto G, Molinari A. (2015) Liposomes as nanomedical devices. Int J Nanomedicine, 10:975–999. [PubMed: 25678787]
26. Christian DA, Cai S, Bowen DM, Kim Y, Pajerowski D, Discher DE. (2009) Polymersome Carriers: from Self-Assembly to siRNA and Protein Therapeutics Eur. J. Pharm. Biopharm 71, 463–474. [PubMed: 18977437]
27. Bangham AD, Horne RW. (1964) Negative Staining of Phospholipids and Their Structural Modification by Surface-Active Agents as Observed in the Electron Microscope. J. Mol. Biol 8: 660–668. [PubMed: 14187392]
28. Papakostas D, Rancan F, Sterry W, Blume-Peytavi U, Vogt A. (2011) Nanoparticles in Dermatology Arch. Dermatol Res 303: 533–500 [PubMed: 21837474]
29. Cui ZK, Bouisse A, Cottenye N, Lafleur M. (2012) Formation of pH-Sensitive Cationic Liposomes from a Binary Mixture of Monoalkylated Primary Amine and Cholesterol. Langmuir. 28: 13668–13674. [PubMed: 22931455]
30. Husseini GA, Pitt WG. (2008) Micelles and Nanoparticles for Ultrasonic Drug and Gene Delivery Adv. Drug Delivery Rev 60: 1137–1152.
31. Soleimani M, Nadri S. (2009) A protocol for isolation and culture of mesenchymal stem cells from mouse bone marrow. Nat Protoc. 4(1):102–6. [PubMed: 19131962]

32. Fan J, Im CS, Guo M, Cui ZK, Fartash A, et al. (2016) Enhanced Osteogenesis of Adipose-Derived Stem Cells by Regulating bone morphogenetic protein signaling antagonists and agonists. Stem Cells Transl Med. 5:539–51. [PubMed: 26956209]
33. Fan J, Im CS, Cui ZK, Guo M, Bezouglaia O, et al. (2015) Delivery of phenamil enhances BMP-2-induced osteogenic differentiation of adipose-derived stem cells and bone formation in calvarial defects. Tissue Eng Part A. 21:2053–65. [PubMed: 25869476]
34. Tournier P, Guicheux J, Paré A, Veziers J, Barbeito A, et al. (2021) An Extrudable Partially Demineralized Allogeneic Bone Paste Exhibits a Similar Bone Healing Capacity as the "Gold Standard" Bone Graft. Front Bioeng Biotechnol. 9:658853. [PubMed: 33968916]
35. Lee S, Park H, Oh JS, Byun K, Kim DY, et al. (2023) Hydroxyapatite microbeads containing BMP-2 and quercetin fabricated via electrostatic spraying to encourage bone regeneration. Biomed Eng Online. 22(1):15. [PubMed: 36803418]
36. Lee D, Wufuer M, Kim I, Choi TH, Kim BJ, et al. (2021) Sequential dual-drug delivery of BMP-2 and alendronate from hydroxyapatite-collagen scaffolds for enhanced bone regeneration. Sci Rep. 11(1):746. [PubMed: 33436904]
37. Seeherman HJ, Berasi SP, Brown CT, Martinez RX, Juo ZS, et al. (2019) A BMP/activin A chimera is superior to native BMPs and induces bone repair in nonhuman primates when delivered in a composite matrix. Sci Transl Med. 11(489):eaar4953. [PubMed: 31019025]
38. Brazil DP, Church RH, Surae S, Godson C, Martin F. (2015) BMP signalling: agony and antagony in the family. Trends Cell Biol. 25(5):249–64. [PubMed: 25592806]
39. Takahashi Y, Ohoka N, Hayashi H, Sato R. (2008) TRB3 suppresses adipocyte differentiation by negatively regulating PPARgamma transcriptional activity. J Lipid Res. 49(4):880–92. [PubMed: 18187772]
40. Bezy O, Vernochet C, Gesta S, Farmer SR, Kahn CR. (2007) TRB3 blocks adipocyte differentiation through the inhibition of C/EBPbeta transcriptional activity. Mol Cell Biol. 27: 6818–6831. [PubMed: 17646392]
41. Du K, Herzig S, Kulkarni RN, Montminy M. (2003) TRB3: a tribbles homolog that inhibits Akt/PKB activation by insulin in liver. Science. 300:1574–1577. [PubMed: 12791994]
42. Wu M, Wang Y, Shao JZ, Wang J, Chen W, et al. (2017) Cbfβ governs osteoblast-adipocyte lineage commitment through enhancing β-catenin signaling and suppressing adipogenesis gene expression. Proc Natl Acad Sci U S A. 114(38):10119–10124. [PubMed: 28864530]
43. Durham EL, Howie RN, Hall S, Larson N, Oakes B, et al. (2018) Optimizing bone wound healing using BMP2 with absorbable collagen sponge and Talymed nanofiber scaffold. J Transl Med. 16(1):321. [PubMed: 30463618]
44. Li C, Samulski RJ. (2020) Engineering adeno-associated virus vectors for gene therapy. Nat Rev Genet. 21(4):255–272. [PubMed: 32042148]
45. Santiago-Ortiz JL, Schaffer DV. (2016) Adeno-associated virus (AAV) vectors in cancer gene therapy. J Control Release. 240:287–301. [PubMed: 26796040]
46. Stender S, Murphy M, O'Brien T, Stengaard C, Ulrich-Vinther M, et al. (2007) Adeno-associated viral vector transduction of human mesenchymal stem cells. Eur Cell Mater. 13:93–9. [PubMed: 17538898]
47. Allen TM, Cullis PR. (2013) Liposomal drug delivery systems: from concept to clinical applications. Adv Drug Deliv Rev. 65(1):36–48. [PubMed: 23036225]
48. Cui Z, Sun J, Baljon J, Fan J, et al. (2017) Simultaneous delivery of hydrophobic small molecules and siRNA using Sterosomes to direct mesenchymal stem cell differentiation for bone repair. Acta Biomater. 58:214–224. [PubMed: 28578107]
49. Drake M, Clarke B, Khosla S. (2008) Bisphosphonates: Mechanism of Action and Role in Clinical Practice. Mayo Clinc Proc. 83(9):1032–1045.
50. Wang G, Babadağli ME, Uludağ H. (2011) Bisphosphonate-Derivatized Liposomes to Control Drug Release from Collagen/Hydroxyapatite Scaffolds. Molecular Pharmaceutics. 8(4):1025–34. [PubMed: 21557579]
51. Pignatello R, Cenni E, Micieli D, Fotia C, Salerno M, Granchi D, et al. (2009) A novel biomaterial for osteotropic drug nanocarriers: synthesis and biocompatibility evaluation of a PLGA-ALE conjugate. Nanomedicine (Lond). 4(2):161–75. [PubMed: 19193183]

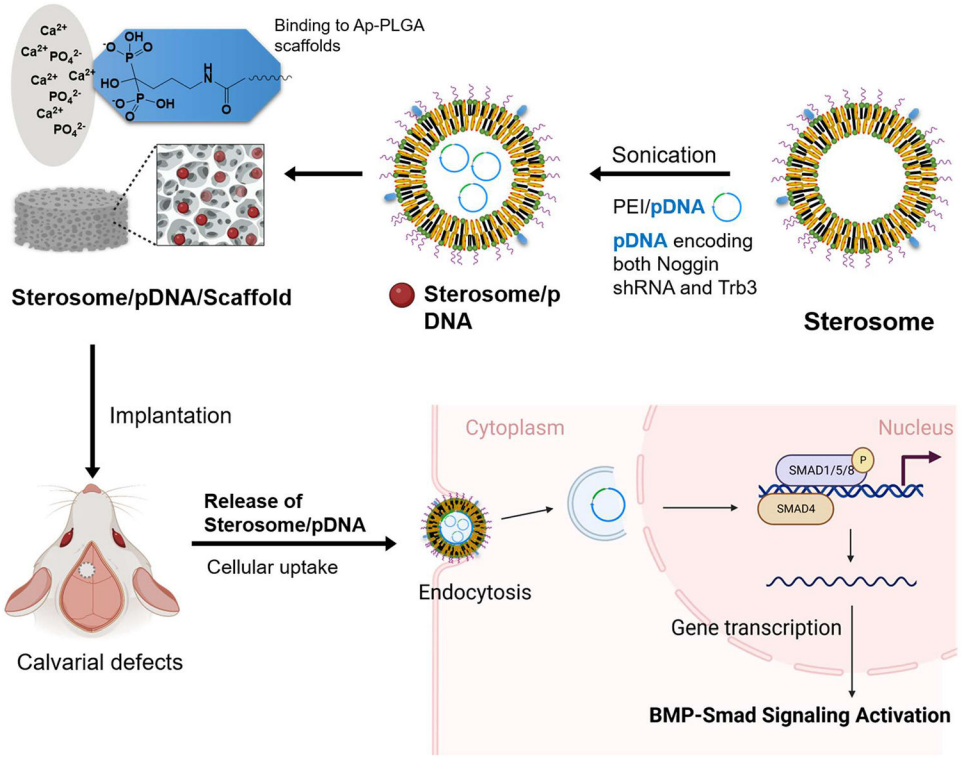

Figure 1:

Schematic diagram of developing sterosome-laden scaffold for bone defect repair through complementary modulation of BMP signaling. The schematic diagram was created with BioRender.com.

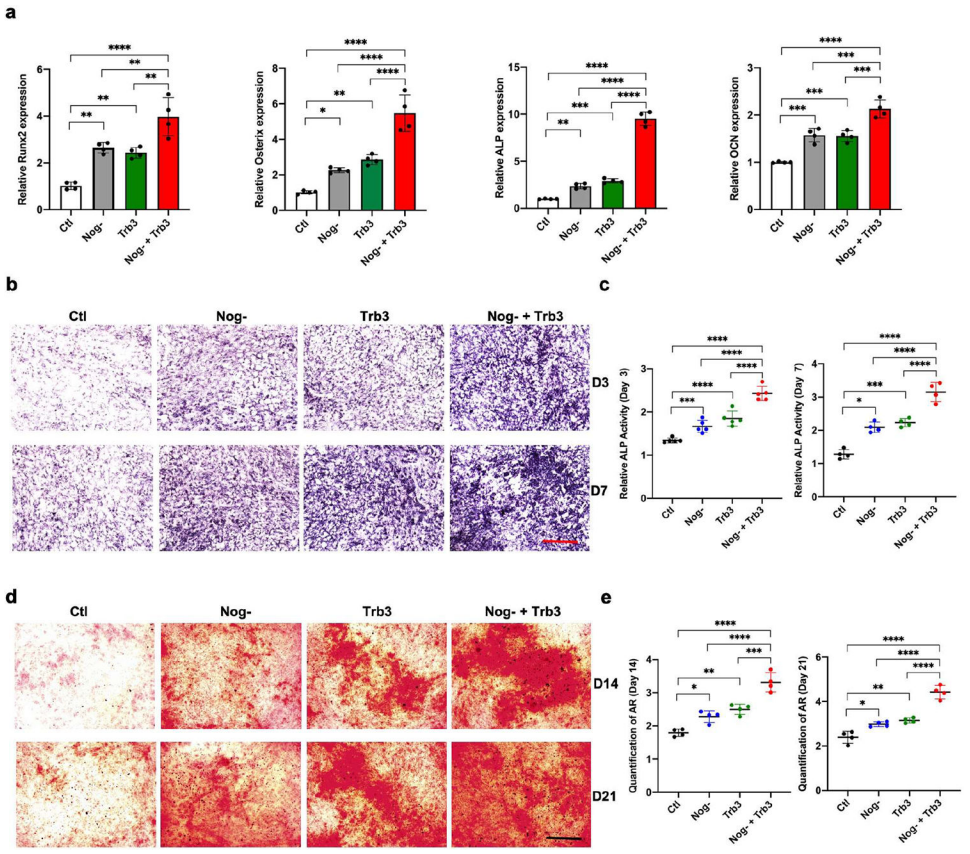

Figure 2: Noggin suppression and Trb3 overexpression enhance osteogenesis in MSCs *in vitro*. Osteogenic markers were examined in mMSCs transduced with lentiviral particles encoding noggin shRNA + Trb3, Trb3, noggin shRNA, or control. (a): The expression of osteogenic genes, including *Runx2, Osterix, ALP*, and *OCN*, was analyzed by a real-time PCR assay at 48 hours, showing upregulation of all genes in cells treated with noggin shRNA + Trb3. (b,c): ALP expression and activity were measured by ALP staining at day 3 and 7. (d,e): Extracellular matrix mineralization was increased in cells with noggin shRNA + Trb3, as demonstrated by alizarin red staining and quantification at day 14 and 21. Data are presented as means ± SD, with significant differences indicated by *, **, ***, and **** ($p < .05$, $p < .01$, $p < .001$, and $p < .0001$, respectively) versus control. Ctl, control; Nog, noggin; AR, alizarin red.

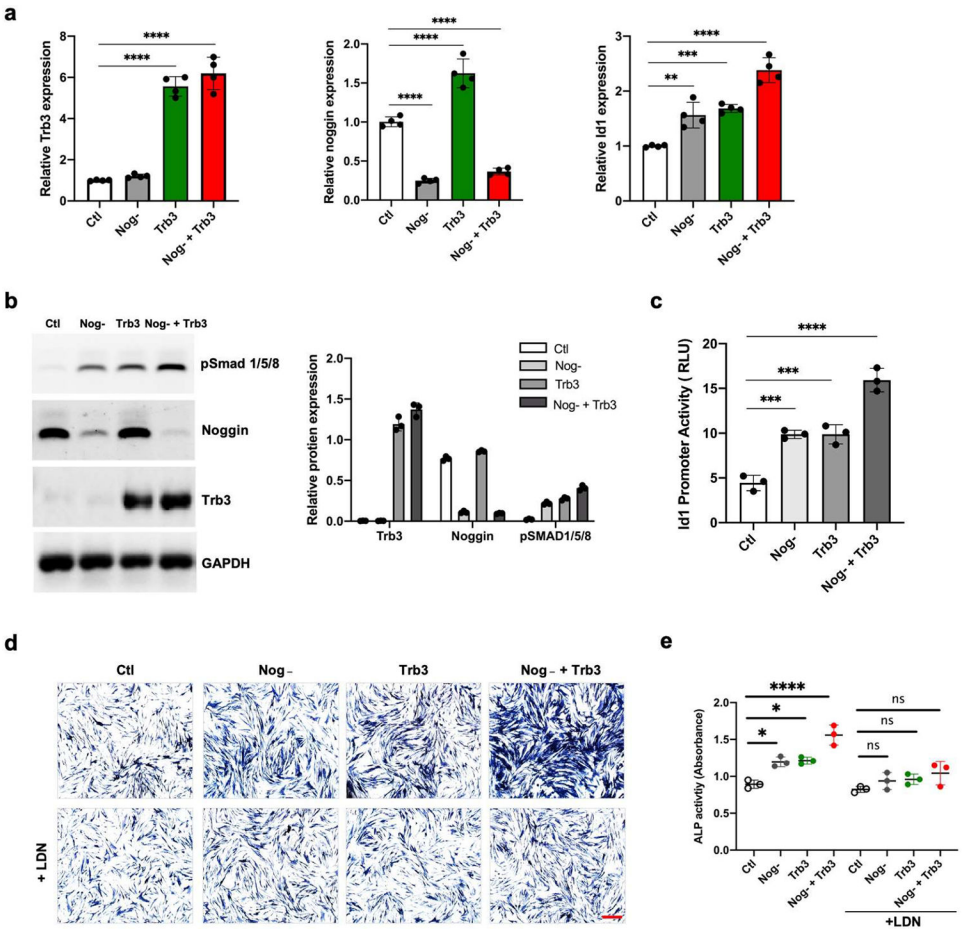

Figure 3: Noggin suppression and Trb3 overexpression stimulate BMP/Smad signaling in mMSCs.

(a): Real-time PCR analysis shows downregulation of noggin and upregulation of Trb3 expression in mMSCs treated with noggin suppression and Trb3 overexpression, leading to significantly increased expression of Id1. (b): Western blot analysis and quantitative data show decreased Noggin expression and increased Trb3 expression, as well as increased phosphorylation of Smad 1/5/8 at 24 hours. (c): Id1 promoter activity is significantly increased in mMSCs treated with noggin suppression and Trb3 overexpression, as measured by luciferase assay. (d,e): ALP activity, a marker of osteogenic differentiation, is significantly increased in mMSCs treated with noggin suppression and Trb3 overexpression, compared to control, and is inhibited by treatment with the BMP signaling inhibitor LDN193189. Scale bar = 2mm. Data are presented as means ± SD. *, $p < 0.05$; **, $p < 0.01$; ***, $p < 0.001$; ****, $p < 0.0001$ versus control. Ctl, control; Nog, noggin; LDN, LDN193189.

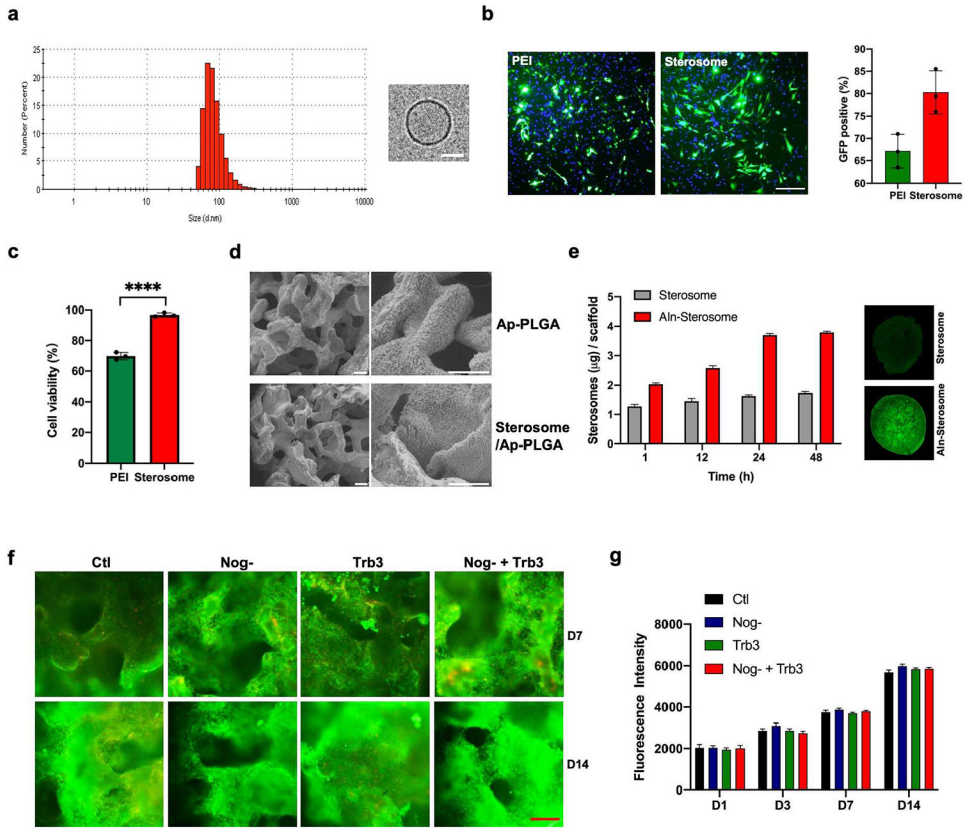

Figure 4: Characterization of Sterosome/Ap-PLGA scaffolds.

(a): Size distribution and TEM image of sterosomes. Scale bar: 50 nm. (b): Transfection efficiency of sterosomes. Fluorescent images of MSCs transfected with pGFP using PEI or sterosomes at 48 h post-transfection. Percentage of GFP positive cells (right). (c): Cell viability of mMSCs transfected with PEI or sterosomes was measured by alamarBlue assay. (d): Scanning electron microscopic (SEM) images of Ap-PLGA scaffolds and Sterosome/Ap-PLGA scaffold. Scale bar: 100 μm. (e): Binding content of sterosomes on Ap-PLGA scaffolds was determined after treatment with sterosomes with or without alendronate (Aln) modifications over 48 h. Fluorescent images of sterosomes bound scaffolds at 24 h (right). (f): Proliferation of mMSCs in the Sterosome/Ap-PLGA scaffolds was assessed by Live-Dead fluorescent staining at days 7 and 14. Scale bar = 500 μm. (g): The MSC proliferation was quantified with alamarBlue assay at days 1, 3, 7, and 14. Ctl, control; Nog, noggin. Data are presented as means ± SD. ****, $p < 0.0001$ versus control.

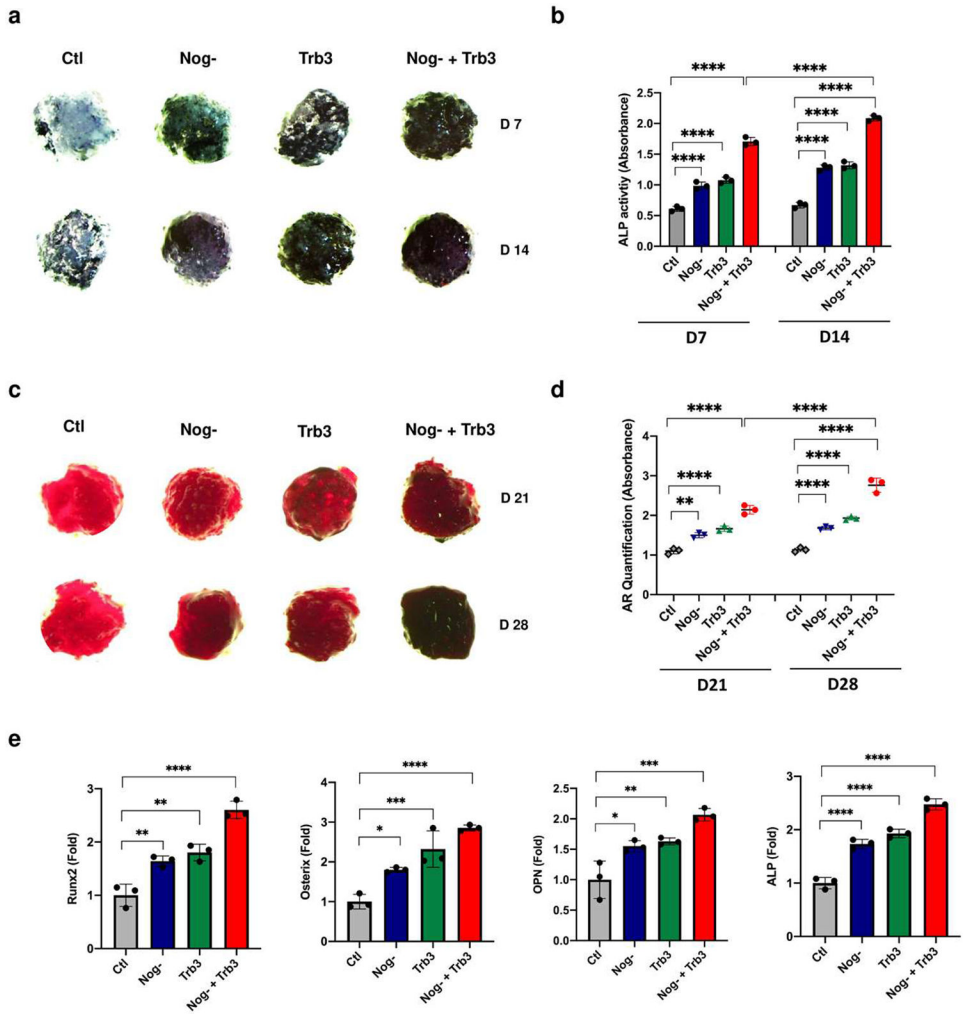

Figure 5: Osteoinduction of Sterosome/Scaffold *in vitro*.

(a,b): ALP expression of mMSCs on the Ap-PLGA scaffold with Sterosome with control, noggin suppression, Trb3 overexpression and noggin suppression + Trb3 overexpression was measured by ALP stain/activities. (c,d): Mineral deposition assessed by Alizarin Red stain. (e): Expression of osteogenic genes including *Runx2, Osterix, OPN* and *ALP*. Data are presented as means ± SD. *, $p < 0.05$; **, $p < 0.01$; ***, $p < 0.001$; ****, $p < 0.0001$ versus control. Ctl, control; Nog, noggin, AR, Alizarin Red stain.

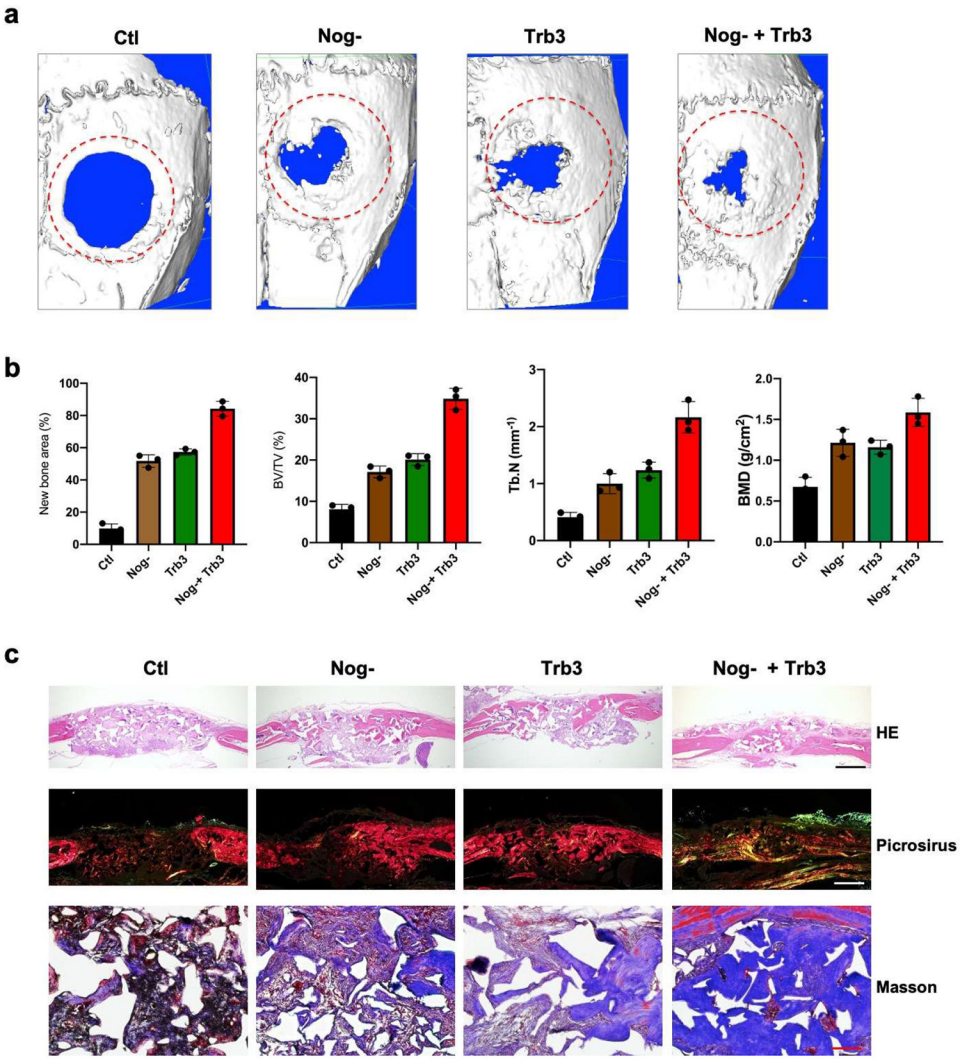

Figure 6: *In vivo* evaluation of bone repair in a calvarial defect model.

(a): MicroCT images of calvarial defects. The red area with a 3-mm diameter indicates the defect site. (b): Semiquantitative analysis of relative new bone area, BV/TV, Tb.N, and BMD. (c): Histological analyses of H&E, Picrosirus red, and Masson trichrome stain. Scale bar = 500 μm (H&E and Picrosirus red), scale bar = 100 μm (Masson stain).

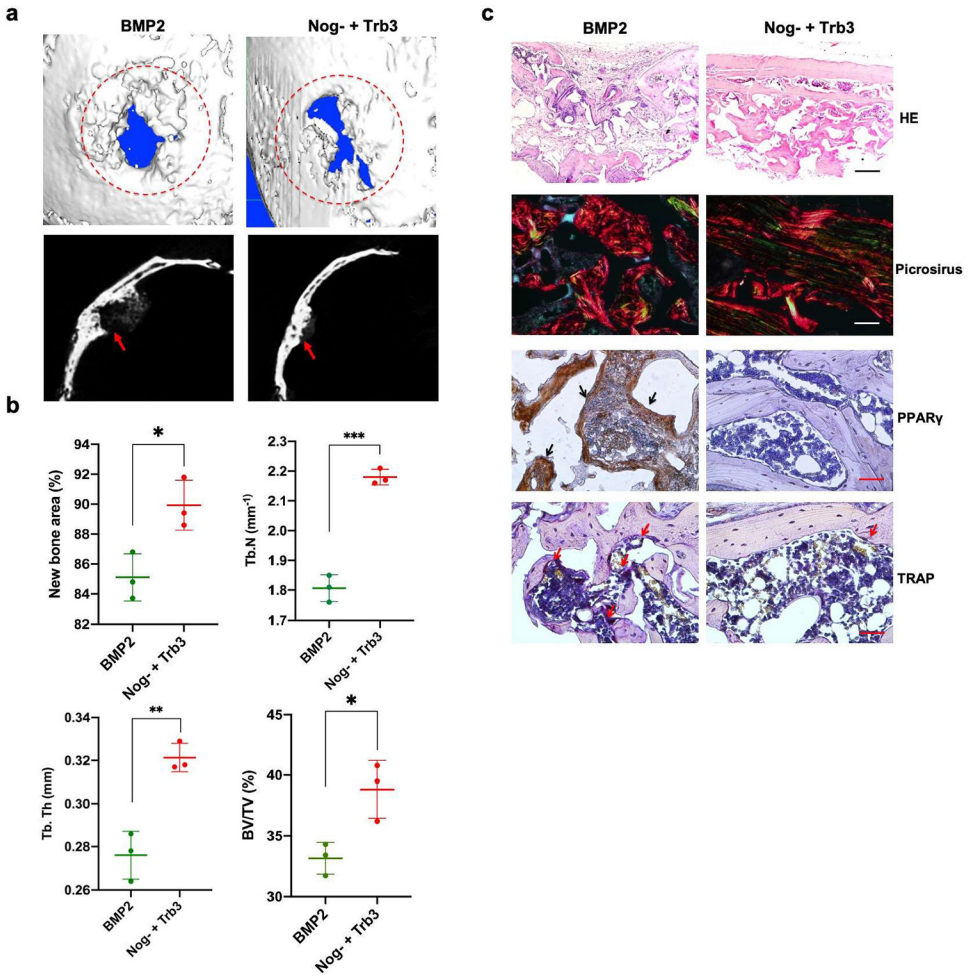

Figure 7: Bone healing in the treatment of BMP2 and Sterosome/scaffold.

(a): microCT images of calvarial defects. The red area with 3-mm diameter indicates the defect site. Red arrow indicates the region of new bone formation. (b): Semiquantitative analysis of relative new bone area, BV/TV, Tb.N, and Tb.Th. (c): Histological analysis of H&E, Picrosirus red stain, immunohistochemical stain of PPARγ and TRAP stain. Black arrow indicates the PPARγ-stained adipocytes. Red arrow indicates the osteoclast. Scale bar = 500 μm (HE), Scale bar = 100 μm (Picrosirus, immunohistochemical stain and TRAP stain). Data are presented as means ± SD. *, $p < 0.05$; **, $p < 0.01$; ***, $p < 0.001$ versus control.